Using Optimal Estimation to Retrieve Winds from VAD Scans by a Doppler Lidar

Sunil Baidar[1,2], Timothy J. Wagner[3], David D. Turner[4], W. Alan Brewer[2]

[1]Cooperative Institute for Research in Environmental Sciences, University of Colorado Boulder, Boulder, CO 80309, USA
5 [2]Chemical Sciences Laboratory, National Oceanic and Atmospheric Administration, Boulder, Colorado 80305 USA
[3]Space Science and Engineering Center, University of Wisconsin-Madison, Madison, Wisconsin 53706 USA
[4]Global Systems Laboratory, National Oceanic and Atmospheric Administration, Boulder, Colorado 80305 USA

Correspondence to: Sunil Baidar (sunil.baidar@noaa.gov)

10 **Abstract.** Low-powered commercially-available coherent Doppler lidar (CDL) provides continuous measurement of vertical profiles of wind in the lower troposphere, usually close to or up to the top of the planetary boundary layer. The vertical extent of these wind profiles is limited by the availability of scatterers, and thus varies substantially throughout the day and from one day to the next. This makes it challenging to develop continuous products that rely on CDL-observed wind profiles. In order to overcome this problem, we have developed a new method for wind profile retrievals from CDL that
15 combines the traditional velocity-azimuth display (VAD) technique with optimal estimation (OE) to provide continuous wind profiles up to 3 km. The new method exploits the level-to-level covariance present in the wind profile to fill in the gaps where the signal to noise ratio of the CDL return is too low to provide reliable results using the traditional VAD method. Another advantage of the new method is that it provides the full error covariance matrix of the solution and profiles of information content, which more easily facilitates the assimilation of the observed wind profiles into numerical weather
20 prediction models. This method was tested using CDL measurements at the Atmospheric Radiation Measurement (ARM) Southern Great Plains (SGP) Central Facility. Comparison with the ARM operational CDL wind profile product and collocated radiosonde wind measurements shows excellent agreement ($R^2 > 0.99$) with no degradation in results where the traditional VAD provided a valid solution. In the region where traditional VAD do not provide results, the OE wind speed has uncertainty of 4.5 m/s. As a result, the new method provides additional information over the standard technique and
25 increases the effective range of existing CDL systems without the need for additional hardware.

1 Introduction and Background

The kinematic profile of the planetary boundary layer (PBL) has a significant impact on disciplines throughout the atmospheric sciences. Low-level wind shear can determine storm mode (e.g. Davies and Johns, 1993) and has significant impacts on aviation safety (e.g. Thobois et al., 2018), while knowledge of the wind profile within the PBL is a significant
30 factor in siting wind energy installations (Banta et al., 2013). High-temporal resolution observations of the wind profile are

crucial for understanding numerous atmospheric processes. While radiosondes remain the standard by which all profiling measuring systems are evaluated, they are not well-suited toward capturing the evolution of boundary layer wind profiles due to their substantial cost per observation and significant time required to prepare and execute each observation. Alternative ways of observing atmospheric wind profiles have been developed, including active remote sensing with radars,

35 lidars, and sodars; passive remote sensing with satellites; and in situ observations with commercial aircraft or uncrewed aircraft systems (UAS).

To address the need for rapid sampling of the wind profile in the PBL, manufacturers have developed low-powered commercial coherent Doppler lidar (CDL) wind profilers. These systems feature turnkey operation, are quick and easy to deploy, and have the ability to run unattended for significant periods of time. Fundamentally, Doppler lidars measure the

40 velocity of scatterers along the emitted beam (radial velocity or line of sight velocity, LOSV); it is assumed that the one-dimensional speed of the scatterers is the same as the wind speed along that direction since the primary scatterers are aerosols. Observations of the vertical profile of the horizontal or three-dimensional wind vector can be retrieved from CDL-observed radial velocities using techniques like velocity-azimuth display (VAD) or Doppler beam swinging (DBS). In both of these techniques, lidar stares along multiple non-coplanar angles are used to reconstruct the vertical profile of the wind

45 vector under the assumption that winds are horizontally homogeneous within the volume observed by the lidar and that they do not evolve during the period (usually a minute or less) in which a set of scans is collected. Numerous studies comparing Doppler lidar wind profile retrievals to in situ observations from radiosondes or instrumented towers and masts have shown that CDLs are a reliable and effective way of measuring wind profiles in the PBL (e.g. Choukulkar et al., 2017; Klein et al., 2015).

50 While the theoretical maximum range of CDLs is 10 km or more and is only limited by the pulse repetition frequency of the emitter and the number of range gates in the detection system, the need for the signal to be scattered and returned to the lidar means that the effective range is much less. CDLs usually feature a laser emitting at 1.5 μm. This wavelength is short enough to be sensitive to aerosols, cloud droplets, and some precipitation, but not so short that it is significantly impacted by molecular scattering. This means it can be a challenge to obtain wind observations at times and heights where aerosol

55 content is low, such as above the top of the PBL. In practice, CDL-observed wind profiles usually extend to 1-2 km above ground level (AGL). While this observation depth is more than sufficient for wind energy applications, other processes such as PBL entrainment or mesoscale dynamics extend to higher altitudes and are difficult to assess with operational CDL retrievals. Furthermore, since the aerosol concentration is not constant, the maximum effective height of CDL-observed wind profiles varies substantially throughout the day and from one day to the next. This makes it challenging to develop

60 continuous products that rely on CDL profiles as the valid range is constantly changing.

In the present work, we propose an alternate method of retrieving wind profiles from CDL observations that combines the traditional VAD technique with optimal estimation (Rodgers, 2000). This exploits the level-to-level covariance present in the wind profile to help fill in the gaps where the signal to noise ratio (SNR) of the lidar return is not strong enough perform the traditional VAD technique. The output of this retrieval technique is a near-continuous profile of winds up to 3 km AGL that

65   agrees very strongly with the traditional VAD at times and heights where both are available, yet still exhibits strong
agreement with radiosondes at heights where the traditional VAD technique was unable to produce a valid result. The
remainder of this paper discusses the retrieval methodology (Sect. 2), compares its performance against both the traditional
VAD and collocated radiosondes (Sect. 3), and offers recommendations and conclusions (Sect. 4).

2 Methodology

2.1 Traditional VAD Method (VADtrad)

In the traditional VAD method (VADtrad), horizontal winds are retrieved from scanning CDL plan position indicator (PPI)
or step-stare scans at one or multiple elevation angles (EAs) using the VAD algorithm described by Browning and Wexler
(1968). The measured radial velocity y_r, at a given range gate r is related to the three-dimensional wind velocity vector x_r by
the viewing geometry. Assuming a horizontally homogeneous wind flow and constant vertical velocity over the sampling
75   volume, a sinusoid is fitted to the radial velocity data at a given range gate (or range bin) to retrieve the wind velocity
components. The wind speed, wind direction and vertical velocity are provided by the amplitude, phase, and offset of the
sinusoid, respectively. Details of VADtrad retrievals and wind precision estimates from a CDL can be found in Newsom et
al. (2017).

2.2 Optimal Estimation VAD Method (VADoe)

80   Wind velocity components are retrieved one range gate at a time and hence one height at a time from a set of line of sight
measurements from an azimuthal scan at a given range gate with the VADtrad technique. While this level-by-level retrieval
can filter out individual bad radial velocity data at each level by applying SNR thresholds or multiple passes of the sinusoidal
fit to determine outliers, it ignores the level-to-level correlation in wind velocity that exists in the atmosphere, information
that can be used to inform about the characteristics of the wind profile further away from the surface. Figure 1 shows the
85   correlation matrices for the u and v component of wind vectors calculated from radiosonde measurements at the Atmospheric
Radiation Measurement (ARM) Southern Great Plains (SGP, Sisterson et al., 2016) Central Facility (C1) in north-central
Oklahoma for the month of July. These correlations were calculated from covariance matrices compiled from 15 years of
radiosonde data (2004-2019) from the ARM facility (SONDEWNPN, 2001), which usually launches radiosondes every six
hours. Since the correlation matrices are symmetric about the diagonal, the lower-right half of the panels in Fig. 1 have been
90   replaced with the correlation matrix for a single representative retrieval for a clear-sky day in July 2019 (to be discussed
later). It is clear that very strong correlations in the prior dataset (i.e., above the diagonal in Fig. 1) exist for wind
components at adjacent heights, while heights that are separated by hundreds of meters still exhibit correlations of 0.5 or
more. This information can be used to assist in retrieving the wind profile at higher altitudes where the lidar SNR is low,
provided that a sufficient number of observations are available from other sources, such as radiosondes or aircraft, to
95   generate the covariance matrices.

One way of integrating the level-to-level correlations with CDL radial velocity observations to produce continuous wind profiles is through the implementation of an optimal estimation retrieval (OE, Rodgers, 2000). In optimal estimation, a set of measurements y is related to the state vector x, which contains parameters describing the current atmospheric state, by a forward model F:

100
$$y = F(x, b) + \epsilon \tag{1}$$

where b represents model parameters that are not retrieved and ϵ represents the model error. In essence, the forward model maps the state of the atmosphere to a set of variables that can be observed directly and contains the physical and instrumental factors that describe the measurements. For many remote sensing applications, the forward model is a radiative transfer model that converts the state of the atmosphere (such as profiles of temperature, water vapor, and trace gases) to radiances at

105 various wavelengths measured by satellites or ground-based radiometers. Through the optimal estimation technique, this relationship is inverted so that a set of observations can be used to obtain the atmospheric state. The optimal estimation technique has been extensively used for retrievals of atmospheric constituent profiles from passive remote sensing measurements where the problem is generally ill-determined (e.g. Kuang et al., 2002; Maahn et al., 2020; Turner and Blumberg, 2019; Turner and Löhnert, 2014). Since ill-determined problems can produce an infinite number of solutions, *a*

110 *priori* information in the form of the mean and covariance of the state vector is used as a constraint to help the algorithm obtain a solution that is both physically possible and statistically likely to occur for a particular location and time of year.

In the present case, in which scanning CDL measurements of radial velocities at different azimuth (α) and elevation (θ) angles are being used to obtain the components of the wind vector (u, v, and w), the forward model is simply the geometry of the measurement that maps the wind vector to the radial coordinate system. It is given by:

115
$$F = [sin\theta \cdot cos\alpha \quad cos\theta \cdot cos\alpha \quad sin\alpha] \tag{2}$$

If one assumes that the vertical velocity, w is much smaller than the horizontal velocity then the contributions of w to the radial wind vector can be neglected. The forward model then reduces to:

$$F = [sin\theta \cdot cos\alpha \quad cos\theta \cdot cos\alpha \quad] \tag{3}$$

Since the forward model F is independent of the state vector x, the jacobian K of the forward model F with respect to the

120 elements of the state vector $x = [u, v]$ is also the forward model

$$K = \frac{dF}{dx} = F \tag{4}$$

Equation (1) can then be linearized as

$$y = Kx + \epsilon \tag{5}$$

The maximum a posteriori solution for Eq. (5) is

125
$$x = x_a + (K^T S_\epsilon^{-1} K + S_a^{-1})^{-1} K^T S_\epsilon^{-1} (y - Kx_a) \tag{6}$$

where x_a is the *a priori* profile and S_a and S_ϵ are the *a priori* and measurement error covariance matrices, respectively. The VADoe retrievals are performed on a fixed vertical resolution defined by the range gate size of the DL measurement. Note that Eq. (5) has an analytical solution, which is the VADtrad result, but provides an unreasonable solution when

measurement SNR is low. This is the reason the VADtrad algorithm is performed layer-by-layer and a SNR threshold is

130   applied. Since the present work evaluates the VADoe retrieval at the ARM SGP Central Facility, the *a priori* information is

calculated from 15 years of profiles of wind speed and direction observed by radiosondes launched at that site to create

monthly mean u and v profiles (x_a) and covariances (S_a). By using monthly *a priori* information instead of a single priori

dataset that spans all seasons for all retrievals, natural variation in the winds can be captured. Few locations will have the in

situ observational density that the ARM SGP site does, but alternate sources of *a priori* data could include Airborne

135   Meteorological Data Relay (Moninger et al., 2003) observations or model output.

Radial velocity uncertainty (σ_r) for a range gate is estimated by calculating the mean of the variance of radial velocity over

two neighboring range gates for each azimuthal stare. For a VAD scan with n azimuth angles, the radial velocity uncertainty

for the jth range gate is given by

$$\sigma_r^2(r_j) = \frac{1}{3n}\sum_{i=1}^{i=n}\sum_{k=j-1}^{j+1}\left(y_r(\theta_i, r_k) - \overline{y}_r(\theta_i, r_j)\right)^2 \tag{7}$$

140   where

$$\overline{y}_r(\theta_i, r_j) = \frac{1}{3}\sum_{k=j-1}^{k=j+1} y_r(\theta_i, r_k) \tag{8}$$

This formulation is similar to the Trial 2 radial velocity uncertainty formulation given in Newsom et al. (2017), where radial

velocity uncertainty is calculated over consecutive scans and neighboring range gates. This formulation was found to result

in the best agreement between wind speed and direction precision estimates from the VADtrad algorithm and sonic

145   anemometer measurements from the collocated 300 m tower at the Boulder Atmospheric Observatory during the

eXperimental Planetary boundary-layer Instrument Assessment (XPIA) field campaign (Lundquist et al., 2017). Unlike

Newsom et al. (2017), the formulation given by Eq. (7) assumes isotropy in atmospheric variance for a given range gate.

Because Eq. (7) assumes isotropy and ignores SNR dependency of measurement uncertainty, the instrument noise

component σ_n is added to σ_r to compute total measurement error. Figure 2 shows the CDL radial velocity precision as a

150   function of SNR determined from ARM SGP C1 Doppler lidar vertical stare measurements using the method described in

Lenschow et al. (2000) and available as part of the standard ARM vertical velocity statistics dataset (Newsom, R. K.,

Sivaraman, C., Shippert, T. R., Riihimaki, 2019a).

The total measurement error variance σ_ϵ for a given viewing geometry i used for constructing the measurement error

covariance matrix is then given by

155    $$\sigma_{\epsilon_i}^2 = \sigma_r^2 + \sigma_{n_i}^2 \tag{9}$$

Both the maximum possible σ_r and σ_n are limited by the CDL measurement bandwidth (±19 m/s for the SGP lidar) and is

much smaller in magnitude than the variability described by the *a priori* covariance (see Fig. 1). This results in the

measurement being artificially weighted higher even when the measurement has little to no information (region to the left of

the dashed vertical line in Fig. 2). In order to overcome this, σ_n are set to a large number (100 m/s) for SNR below 0.005 (~-

160   23 dB). This value needs to be optimized depending upon the number of azimuth beams used in the retrieval. The non-

diagonal elements were set to 0, assuming there was no correlation between the uncertainties at different range gates and different azimuth angles.

The solution given by Eq. (6) is a weighted mean of the *a priori* profile and the information from the measurement. The weight is given by the averaging kernel matrix A,

165 $$A = (K^T S_\epsilon^{-1} K + S_a^{-1})^{-1} K^T S_\epsilon^{-1} K \qquad (10)$$

The retrieval at any range gate is an average of the whole profile weighted by the row of the averaging kernel matrix corresponding to that range gate. The A matrix also can be used to determine the number of independent pieces of information retrieved (often quantified as the degrees of freedom, or DOF) as well as an estimate of the vertical resolution of the retrieved profile at a given level. Note that in a traditional VAD level-by-level retrieval, each range gate is considered as

170 independent and the range gate resolution defines the vertical resolution of retrieved profiles. For an ideal retrieval scenario, A is the identity matrix, the DOF equals the number of retrieved profile layers and the averaging kernels peak at their corresponding altitudes. In reality, the retrieved profile is a smoothed version of the true profile. In case of the scanning CDL measurements, A is close to an identity matrix throughout most of the PBL where the SNR is relatively high. As a result, the *a priori* provides minimal to no constraint at those altitudes. However, at altitudes where measurement SNR is low, the

175 VADoe retrieval is capable of providing an *a priori*-constrained retrieval, even below the SNR threshold usually applied to VAD retrievals.

One of the advantages of the optimal estimation technique is that uncertainties from both the instrument and the retrieval are propagated throughout the process so an overall error for each individual observation can be easily quantified. The posterior error covariance matrix which includes contributions from smoothing error and measurement error is given by

180 $$S_{op} = (S_a^{-1} + K^T S_\epsilon^{-1} K)^{-1} \qquad (11)$$

An additional source of uncertainty is the accuracy of the forward model, which is affected by the assumption of horizontally homogeneous wind flow, isotropic turbulence and vertical velocity component is negligible. This forward model error is given by

$$S_f = G_y \Delta f^2 G_y^T = G_y [f(x, b, b') - F(x, b)]^2 G_y^T \qquad (12)$$

185 where $G_y = AK$ is the gain matrix, f is the idealized forward model which includes all the correct physics and F is the simplified approximation. In an ideal scenario, $f(x, b, b') = y$. Therefore, we calculated forward model error as

$$S_f = G_y \Delta f^2 G_y^T = G_y [y - Kx]^2 G_y^T \qquad (13)$$

The total retrieval error covariance S_{total} is given by

$$S_{total} = S_{op} + S_f \qquad (14)$$

190 The square root of the diagonal element of S_{total} provides the 1-σ uncertainty for the retrieved *u* and *v* profiles.

3 Results

ARM operates a total of 5 CDLs at the SGP site: one Halo Streamline XR at the C1 facility and four Halo Streamlines (Pearson et al., 2009) at extended facilities that surround the C1 site at a distance of approximately 50 km. Each ARM CDL makes near-continuous measurements of radial velocity and attenuated backscatter coefficient profiles at a wavelength of 1.5

195 μm. These CDLs are sensitive to aerosols but not molecular backscatter and hence the measurements are confined to the PBL. Details about the ARM Doppler lidars, their operations, and data products are found in Newsom and Krishnamurthy (2020). We used the CDL measurements at the SGP C1 (DLPPI, 2010) for this study. The Doppler lidar at the SGP C1 site that is further examined in this work operates with 30 m range gate resolution and 1.3 s time resolution. It is typically configured to perform one 8-beam PPI scan at a 60 degree elevation angle every 15 minutes and performs vertical stares

200 during the remaining time. The PPI scan takes approximately 40 seconds. Horizontal wind profiles are retrieved from the PPI scan using the VAD method. The ARM DL wind retrieval algorithm is described in detail in Newsom et al. (2019b). It employs a SNR threshold of 0.008 (~ -21 dB) to filter out poor-quality radial velocity data before computing wind profiles.

To evaluate the performance of the optimal estimation retrieval against real-world observations, VADoe retrievals from the ARM SGP C1 lidar were processed for the entirety of the 2019 calendar year. Normally, radiosondes are launched

205 from the SGP site four times a day, but the launch frequency was doubled to eight daily sondes for the three-month period lasting from May through July 2019. In all, over 1600 radiosondes were collocated with Doppler lidar profiles during the year-long study period. Each radiosonde was temporally matched to the Doppler lidar profile that was taken nearest in time to the radiosonde launch time. Radiosondes that were launched more than 30 min from the nearest valid lidar observation were excluded from this analysis.

210 An important parameter for evaluating the utility of an optimal estimation retrieval is the information content. One measure of this is the degrees of freedom of the signal (DFS) which can be used to identify how many unique pieces of information are present in the retrieval as well as determine at what altitudes the information can be found. While the OE wind retrieval is output onto a fixed grid with 113 evenly-spaced levels from the surface to 3000 m, the fact that OE-retrieved observations are overlapping weighted averages of various depths in the atmosphere means that there will be fewer

215 than 113 uncorrelated pieces of information in the output. The cumulative DFS of the retrieval at the nth level is the sum of the first n elements of the diagonal of the averaging kernel A (Eq. 10); the total DFS of the retrieval is thus simply the trace of A. Figure 3 shows the mean and standard deviation of the DFS as a function of height for the 1600+ OE wind profiles that were matched to a radiosonde. On average, the total profile DFS is approximately 15 though the variability ranges from 4.9 to 25.3, and the u and v DFS are effectively identical. Most of the DFS are concentrated in the lowest 1000 m, with

220 approximately 10.3 DFS on average below that height which means the true vertical resolution of the DL is around 100 m. True vertical resolution of the DL wind profiles can be improved by including multiple PPI at different EAs and increasing the number of azimuth angles in a PPI scan. However, with roughly 5 DFS in the OE retrieval above 1000 m, the retrieval can still provide valuable information about an otherwise under observed layer of the atmosphere. An advantage of

calculating the cumulative DFS and the related true vertical resolution profiles from the optimal estimation retrieval is that it

225 easily facilitates the assimilation of the observed wind profiles into NWP (Coniglio et al., 2019).

One way to evaluate the performance of the OE winds is by examining a sample plot of the winds as measured by various systems. Figure 4 depicts time-height cross sections of the *v* component of the wind on 16 May 2019. This was a quiescent day at the SGP site with a persistent upper-level ridge ensuring few clouds and little synoptic forcing. These conditions enabled the formation of a low-level jet (LLJ) over the region, with winds approaching 20 m s^{-1} approximately 250 m above

230 the ground at 0600 UTC (1:00 AM local time). Since this was during the period of 3 h radiosonde launches from SGP, enough radiosonde profiles are present to capture some of the short-term variability in the atmospheric state. The VADtrad profiles are limited to heights approximately 1000 m AGL and below. While VADtrad can resolve the LLJ and daytime turbulence in the PBL, an insufficient number of scatterers above those levels means that the VADtrad is incapable of resolving any phenomena at higher altitudes. By contrast, the OE provides continuous profiles from the surface to 3000 m

235 AGL. While the information content is not as large at these higher altitudes as noted previously, the presence of even a few independent data points in the 1500 - 3000 m range can bring new insight to processes in the entrainment zone and free troposphere. For example, the sondes indicate a secondary maximum of *v* winds above the low level jet between 1000 and 2000 m. The 0.008 SNR threshold used operationally by ARM means that this feature is missed entirely by VADtrad. Likewise, in the afternoon hours (after 1900 UTC) the PBL has grown too deep to be fully resolved by the VAD, yet the OE

240 retrieval is able to monitor the continued increase in the depth of the turbulent winds as it allows even regions of low SNR to be used and to have an impact on the retrieved profile. The sondes are able to note the depth of this layer, but the 3 h launch frequency is still too coarse to resolve the individual elements the way the OE retrieval can. OE results in Fig. 4 shows faint vertical striping at higher altitudes where there is little to no information available from DL. This is due to the inherent nature of the VADoe retrieval which includes level-to-level correlation but no time dependent information.

245 To facilitate intercomparisons between the radiosondes and both VADtrad and VADoe, the same grid from the traditional VAD technique was used for the OE output, and the radiosonde observations were interpolated to that grid. As any OE-retrieved variable at a given height represents a weighted average of that variable above and below the observation height, the radiosonde profiles are smoothed according to the following formula:

$$x_{smooth} = A(x_{sonde} - x_a) + x_a \tag{15}$$

250 where A is the averaging kernel for the retrieval and x_a is the mean prior state. For VADtrad/radiosonde comparisons, only unsmoothed sondes are used. Quality control measures included rejecting VAD observations with an absolute value greater than 50 m s^{-1} and OE retrievals where the OE-derived measurement uncertainty exceeded 5 m s^{-1}.

Scatter plots showing the performance of both the traditional VAD-derived CDL wind observations and the OE-retrieved CDL winds throughout the 2019 analysis period are shown in Fig. 5. Several important points emerge from this figure. First,

255 it is important to note that the VAD and OE wind observations are almost identical for the times and heights where both are available as the correlation coefficients between the two sets of CDL observations are 0.998 and 0.999 for the *u* and *v* wind components respectively. In essence, using the VADoe retrieval in place of the VADtrad technique does not degrade the

quality of the observations but instead augments existing observations with additional information at heights above those observed by VADtrad. Second, the VADtrad winds appear to have a stronger correlation with the radiosondes than the

260 VADoe winds do at first glance. However, the OE winds include many observation points where the traditional technique does not provide an observation. A more appropriate analysis limits the intercomparison to only the points that are present in both VADoe and VADtrad. In those cases (depicted with orange points in Fig. 5b and 5e), the sonde/OE correlations are functionally identical to the sonde/traditional comparisons and have effectively the same correlation values. This further reinforces the idea that the OE winds can be used in place of the traditional VAD winds without degrading the near-surface

265 observations. Finally, it is worth noting that, regardless of the instruments being compared, correlations are higher for the v component than they are for the u component. This may be due to the fact that the flow over the SGP site is persistently southerly and the u wind tends to be more variable than the v wind. Note that natural variability in winds and turbulence results in an inherent scatter between lidar and sonde wind measurements.

The mean and standard deviation of the lidar-minus-sonde differences at a given observation height can be used to determine

270 the bias and uncertainty present in the lidar observations at that height. Figure 6 shows the vertical profile of the bias (mean difference) and uncertainty (standard deviation of the differences) for both the VADtrad and VADoe profiles relative to the radiosondes throughout the lower troposphere. It is clear that the VADoe retrievals are equal to or better than the VADtrad winds at all analyzed heights, especially at the middle and upper levels. With respect to the u component (Fig. 6a), the two techniques have nearly indistinguishable performance in the lowest 800 m, as both have a slight slow bias that increases

275 from -0.10 at the lowest range gate to -0.38 m s^{-1} at 800 m. The uncertainties slightly increase over that depth, from 1.17 m s^{-1} at the lowest level to 1.54 at 800 m. From 800 m to 1300 m, the bias remains similar for both techniques, but the uncertainty starts to diverge as the VADoe u uncertainty is mostly constant with increasing height while the VADtrad u uncertainty increases with increasing height. Above 1300 m, substantial differences in the performance of the two systems are present. The VADoe u wind show a slight increasingly negative bias with increasing height, but the VADtrad u bias

280 becomes much more negative as height increases. The VADoe u wind bias at 1500 m, 2000 m, and 3000 m is -0.78, -0.90, and -1.34 m s^{-1} respectively; while the VADtrad u bias at those heights is -0.94, -3.14, and -6.12 m s^{-1} respectively. There is similar inflation in the uncertainty with height above 1300 m, as once again the VADoe technique shows only slight increases while the VADtrad uncertainty more than doubles. While the u bias was slow at all depths for both techniques, the v bias is generally fast (Fig. 6b). Like the u bias, the VADoe v bias is small at all heights. It never exceeds 0.9 m s^{-1} at any

285 height while the VADtrad v bias steadily increases throughout the analyzed depth to more than 3.4 m s^{-1} at the highest levels. The VADoe v uncertainties are again approximately the same as the VADtrad v uncertainties at the low levels but show little change with height at the upper levels, while the VADtrad uncertainties increase substantially, going from 2.65 m s^{-1} at 1500 m to 8.86 m s^{-1} at 3000 m. Larger uncertainties for VADtrad relative to VADoe at higher altitudes (> 1500 m) is due to a very small number of data points, which are also very likely bad data points that pass the SNR threshold, included in the

290 comparison. In contrast, the lower uncertainties for VADtrad between 500-1500 m is because of only relatively good data

points being included in the comparison for VADtrad (see Fig. 6c for the number of points included in the comparison at each height).

Figure 6 also shows the number of valid intercomparisons as a function of height by showing the number of valid lidar/sonde intercomparisons for each lidar range gate (Fig. 6c). Here, it is clear how rapidly the number of VADtrad observations

295   decreases with height due to the decreasing concentration of scatterers. At 1 km AGL, the number of observations is only 59% of what it was at the lowest range gate. By comparison, the VADoe retrieval still has 98% of the lowest-level observations. The number of VADoe observations decreases with height due to the imposition of the 5 m s^{-1} gross error check noted earlier, but it is clear that the decrease in the availability of the VADoe product with increasing height is much less than it is for the VADtrad wind profiles.

300   While the retrieval is conducted in terms of u and v, it is instructive to evaluate how the retrieval performs in terms of wind speed and direction. These are presented in Fig. 6d and 6e respectively. The VADtrad and VADoe wind speed biases (Fig. 6d) are remarkably similar with height, increasing from near 0 m s^{-1} adjacent to the surface to approximately -1.5 m s^{-1} at 3 km. Significant differences between the two retrieval techniques are seen in the uncertainties, however. Below 1.5 km AGL, the uncertainties are very similar with VADtrad showing slightly smaller uncertainty. However, above 1.5 km the two

305   uncertainty curves diverge greatly with VADtrad exhibiting more than 50% more uncertainty in this region than VADoe. It is important to note that the 1.5 km level is an approximate representation of the height of the daytime boundary layer at the SGP site and is a height above which there are few VADtrad observations. The vertical profile of direction differences (Fig. 6e) shows that both techniques have effectively identical biases in the lowest 1200 m. Above that height, the VADoe biases remain low while the VADtrad biases become increasingly negative with height. The VADoe has slightly larger

310   uncertainties than the VADtrad up to approximately 1800 m, beyond which they are largely the same.

Since a significant advantage of the OE retrieval is providing observations at altitudes for which no VADtrad data are available at standard values for SNR, it is worth looking specifically at the performance of the observations as a function of SNR. As noted in Fig. 5 and 6, most of the spread in the OE-minus-sonde differences is occurring for the levels where VADtrad observations are not available. Figure 7 illustrates the VADoe minus radiosonde wind speed difference within four

315   different bands of SNR. As noted above, the ARM standard cutoff for SNR is 0.008 which corresponds to approximately -21 dB, and VADoe implements a soft -23 dB cutoff by setting individual LOSV error to 100 m/s for data with SNR below -23 dB. The data are divided approximately evenly into two groups with a higher SNR than the -21 dB cutoff, as well as SNR between -21 and -23 dB, and SNR below -23 dB. In order to minimize the impact of cloud returns, the highest SNR group (> -13 dB) is limited to data from lowest 800 m. Note that CDL SNR is not range corrected and hence absolute SNR threshold

320   cannot be applied to filter for clouds. The best performance is found in the group with SNR between -21 and -13 dB (Panel 7b) as that show smaller bias and standard deviation than other groups. Panel 7c depicts observations with SNR in between the VADtrad and VADoe cutoffs. Bias and uncertainty in the VADoe retrievals in this SNR region are comparable to the groups with better SNR indicating that at least some of the observations in this SNR region might potentially be available from VADtrad method if the SNR cutoff threshold were to be lowered. Nonetheless this also highlights the benefit of the

325 VADoe retrieval where a more liberal SNR cutoff threshold could be applied. Panel 7d shows observations that would not be available for VADtrad retrieval at all. The bias and uncertainty of this group of observations are -2.52 m/s and 4.49 m/s respectively. While the VADoe observations in this SNR bands depict larger biases and greater uncertainty than the observations in better SNR bands, the uncertainty is comparable to the Tropospheric Airborne Meteorological Data Reporting (TAMDAR) system (Wagner and Petersen, 2021), and within the WMO threshold requirement for horizontal

330 wind measurements in the free troposphere for Global and high resolution NWP (WMO, 2022). Considering that only 37.1% of the total dataset evaluated here has an SNR better than -21 dB, the VADoe technique provides many more usable observations.

Figure 8 shows the wind direction differences in the same SNR groupings as Fig. 7. It is interesting to note that in this case the -23 to -21 dB band is actually less biased than both the bands with better SNR, and the uncertainties are comparable.

335 Wind speed in the -13 to 0 dB band also showed higher bias and uncertainty. This is likely due to presence of higher variability in wind and higher turbulence in the lower PBL where the CDL SNR is greatest. Observation of precipitation droplets is another possible reasoning for the higher uncertainty and the tail in the distribution at the highest SNR bin. As expected, both the bias and uncertainty are higher for the SNR less than -23 dB bin.

4 Summary/Conclusion

340 Coherent Doppler lidars have many research, operational, and commercial applications. Through deployments around the world, they have proven to be reliable and robust instruments that have significantly enhanced our understanding of numerous processes and phenomena. However, since commercially available low-powered CDLs operating at 1.5 μm wavelength are insensitive to molecular scattering and thus must rely on aerosol scattering, the vertical extent of the wind profiles they observe is limited to the planetary boundary layer where aerosol concentrations are greatest. However, many

345 key atmospheric processes are found at or above the top of the boundary layer which means that many CDLs are unable to observe them with standard algorithms.

To provide profiles that are more vertically and temporally continuous, an optimal estimation retrieval was created so that established level-to-level correlations can be exploited to gain information about the wind profile at levels higher than those where CDLs can typically reach. This retrieval, called VADoe, is computationally simple as the forward model is derived

350 from simple geometry. Critically, with correlations of 0.998 and 0.999 between the VADtrad and VADoe for the *u* and *v* wind components respectively when both techniques are valid (i.e. the SNR in the observations is sufficient), using an OE retrieval does not degrade the existing retrievals. It merely provides additional information where none is currently available. The VADoe provides useful results, although with higher uncertainty, even when the SNR is too small and radial velocities are not reliable.

355 Optimal estimation retrievals have significant advantages for data assimilation. With well-characterized uncertainties for each observation and profiles of degrees of freedom of the signal and vertical resolution easily obtained as part of the

retrieval, profiles from the VADoe algorithm are ready for assimilation into numerical weather prediction without needing to assume error profiles or other needed characteristics. Further, OE provides a framework for a combined wind profile retrieval from co-located different types of instruments for wind measurements (e.g. CDL, direct detection Doppler lidar, radar).

It is important to note that VADoe can easily be applied to existing instruments and data. So long as the original scan files have been retained, data collected from previous deployments and field campaigns can be reprocessed using this technique to reveal latent information that has not yet been seen. In addition, additional effective range, whose uncertainty is comparable to TAMDAR and meets WMO threshold requirements for wind measurements for high resolution NWP, from existing CDL infrastructure can be realized with no additional capital expense.

Data availability: DL and Sonde data from ARM SGP Central Facility is available via ARM Data Center (https://adc.arm.gov/discovery/#/)

Author contributions: SB, DDT, and WAB developed the retrieval code. SB, TJW and DDT analyzed the data and wrote the manuscript.

Competing interests: The authors declare that they have no conflict of interest.

Acknowledgements: This research was supported in part by NOAA cooperative agreements NA17OAR4320101 and NA22OAR4320151, the U.S. Department of Energy's Atmospheric System Research, an Office of Science Biological and Environmental Research program, under Grant No. DE-SC0020114, and the NOAA Atmospheric Science for Renewable Energy Program.

References

Miller, B. B. and Carter, C.: The test article, J. Sci. Res., 12, 135–147, doi:10.1234/56789, 2015.

Smith, A. A., Carter, C., and Miller, B. B.: More test articles, J. Adv. Res., 35, 13–28, doi:10.2345/67890, 2014.

Atmospheric Radiation Measurement (ARM) user facility: Balloon-Borne Sounding System (SONDEWNPN). 2004-01-01 to 2019-12-31, Southern Great Plains (SGP) Central Facility, Lamont, OK (C1), compiled by K. Burk, ARM Data Center, available at http://dx.doi.org/10.5439/1595321, 2001.

Atmospheric Radiation Measurement (ARM) user facility: Doppler Lidar (DLPPI), 2019-01-01 to 2019-12-31, Southern Great Plains (SGP) Central Facility, Lamont, OK (C1), compiled by R. Newsome and R. Krishnamurthy, ARM Data Center, available at http://dx.doi.org/10.5439/1025186, 2010.

Banta, R. M., Pichugina, Y. L., Kelley, N. D., Hardesty, R. M. and Brewer, W. A.: Wind Energy Meteorology: Insight into Wind Properties in the Turbine-Rotor Layer of the Atmosphere from High-Resolution Doppler Lidar, Bull. Am. Meteorol. Soc., 94(6), 883–902, doi:10.1175/BAMS-D-11-00057.1, 2013.

Browning, K. A. and Wexler, R.: The Determination of Kinematic Properties of a Wind Field Using Doppler Radar, J. Appl. Meteorol., 7(1), 105–113, doi:10.1175/1520-0450(1968)007<0105:TDOKPO>2.0.CO;2, 1968.

Choukulkar, A., Brewer, W. A., Sandberg, S. P., Weickmann, A., Bonin, T. A., Hardesty, R. M., Lundquist, J. K., Delgado, R., Iungo, G. V., Ashton, R., Debnath, M., Bianco, L., Wilczak, J. M., Oncley, S. and Wolfe, D.: Evaluation of single and multiple Doppler lidar techniques to measure complex flow during the XPIA field campaign, Atmos. Meas. Tech., 10(1), 247–264, doi:10.5194/AMT-10-247-2017, 2017.

Coniglio, M. C., Romine, G. S., Turner, D. D. and Torn, R. D.: Impacts of Targeted AERI and Doppler Lidar Wind Retrievals on Short-Term Forecasts of the Initiation and Early Evolution of Thunderstorms, Mon. Weather Rev., 147(4), 1149–1170, doi:10.1175/MWR-D-18-0351.1, 2019.

Davies, J. M. and Johns, R. H.: Some Wind and Instability Parameters Associated With Strong and Violent Tornadoes 1. Wind Shear and Helicity .National Severe Storms Forecast Center, Kansas City, Missouri 64106., 1993.

Klein, P., Bonin, T. A., Newman, J. F., Turner, D. D., Chilson, P. B., Wainwright, C. E., Blumberg, W. G., Mishra, S., Carney, M., Jacacobsen, E. P., Wharton, S. and Newsom, R. K.: LABLE: A multi-institutional, student-led, atmospheric boundary layer experiment, Bull. Am. Meteorol. Soc., 96(10), 1743–1764, doi:10.1175/BAMS-D-13-00267.1, 2015.

Kuang, Z., Margolis, J., Toon, G., Crisp, D. and Yung, Y.: Spaceborne measurements of atmospheric CO2 by high-resolution NIR spectrometry of reflected sunlight: An introductory study, Geophys. Res. Lett., 29(15), 2–5, doi:10.1029/2001gl014298, 2002.

Lenschow, D. H., Wulfmeyer, V. and Senff, C.: Measuring second- through fourth-order moments in noisy data, J. Atmos. Ocean. Technol., 17(10), 1330–1347, doi:10.1175/1520-0426(2000)017<1330:MSTFOM>2.0.CO;2, 2000.

Lundquist, J. K., Wilczak, J. M., Ashton, R., Bianco, L., Brewer, W. A., Choukulkar, A., Clifton, A., Debnath, M., Delgado, R., Friedrich, K., Gunter, S., Hamidi, A., Iungo, G. V., Kaushik, A., Kosovic, B., Langan, P., Lass, A., Lavin, E., Lee, J. C. Y., McCaffrey, K. L., Newsom, R., Noone, D. C., Oncley, S. P., Quelet, P. T., Sandberg, S. P., Schroeder, J. L., Shaw, W. J., Sparling, L., Martin, C. S., Pe, A. S., Strobach, E., Tay, K., Vanderwende, B. J., Weickmann, A., Wolfe, D. and Worsnop, R.: Assessing State-of-the-Art Capabilities for Probing the Atmospheric Boundary Layer: The XPIA Field Campaign, Bull. Am. Meteorol. Soc., 98(2), 289–314, doi:10.1175/BAMS-D-15-00151.1, 2017.

Maahn, M., Turner, D. D., Löhnert, U., Posselt, D. J., Ebell, K., Mace, G. G. and Comstock, J. M.: Optimal estimation retrievals and their uncertainties, Bull. Am. Meteorol. Soc., 101(9), E1512–E1523, doi:10.1175/BAMS-D-19-0027.1, 2020.

Moninger, W. R., Mamrosh, R. D. and Pauley, P. M.: Automated Meteorological Reports from Commercial Aircraft, Bull. Am. Meteorol. Soc., 84(2), 203–216, doi:10.1175/BAMS-84-2-203, 2003.

Newsom, R. K., Krishnamurthy, R.: Doppler Lidar (DL) Instrument Handbook. [online] Available from: https://www.arm.gov/publications/tech_reports/handbooks/dl_handbook.pdf, 2020.

Newsom, R. K., Sivaraman, C., Shippert, T. R., Riihimaki, L. D.: Doppler Lidar Vertical Velocity Statistics Value-Added Product., 2019a.

Newsom, R. K., Sivaraman, C., Shippert, T. R., Riihimaki, L. D.: Doppler Lidar WIND Value-Added Product., 2019b.

425 Newsom, R. K., Alan Brewer, W., Wilczak, J. M., Wolfe, D. E., Oncley, S. P. and Lundquist, J. K.: Validating precision estimates in horizontal wind measurements from a Doppler lidar, Atmos. Meas. Tech., 10(3), 1229–1240, doi:10.5194/amt-10-1229-2017, 2017.

Pearson, G., Davies, F. and Collier, C.: An analysis of the performance of the UFAM pulsed Doppler lidar for observing the boundary layer, J. Atmos. Ocean. Technol., 26(2), 240–250, doi:10.1175/2008JTECHA1128.1, 2009.

430 Rodgers, C. D.: Inverse Methods for Atmospheric Sounding: Theory and Practice, World Scientific., 2000.

Sisterson, D. L., Peppler, R. A., Cress, T. S., Lamb, P. J. and Turner, D. D.: The ARM Southern Great Plains (SGP) Site, Meteorol. Monogr., 57(1), 6.1-6.14, doi:10.1175/AMSMONOGRAPHS-D-16-0004.1, 2016.

Thobois, L., Cariou, J. P. and Gultepe, I.: Review of Lidar-Based Applications for Aviation Weather, Pure Appl. Geophys. 2018 1765, 176(5), 1959–1976, doi:10.1007/S00024-018-2058-8, 2018.

435 Turner, D. D. and Blumberg, W. G.: Improvements to the AERIoe thermodynamic profile retrieval algorithm, IEEE J. Sel. Top. Appl. Earth Obs. Remote Sens., 12(5), 1339–1354, doi:10.1109/JSTARS.2018.2874968, 2019.

Turner, D. D. and Löhnert, U.: Information content and uncertainties in thermodynamic profiles and liquid cloud properties retrieved from the ground-based Atmospheric Emitted Radiance Interferometer (AERI), J. Appl. Meteorol. Climatol., 53(3), 752–771, doi:10.1175/JAMC-D-13-0126.1, 2014.

440 Wagner, T. J. and Petersen, R. A.: On the Performance of Airborne Meteorological Observations against Other In Situ Measurements, J. Atmos. Ocean. Technol., 38(6), 1217–1230, doi:10.1175/JTECH-D-20-0182.1, 2021.

WMO: WMO Observing Systems Capability Analysis and Review Tool (OSCAR): Requirements defined from Wind (horizontal). [online] Available from: https://tools.wmo.int/variables/view/wind_horizontal (Accessed 5 September 2022), 2022.

445
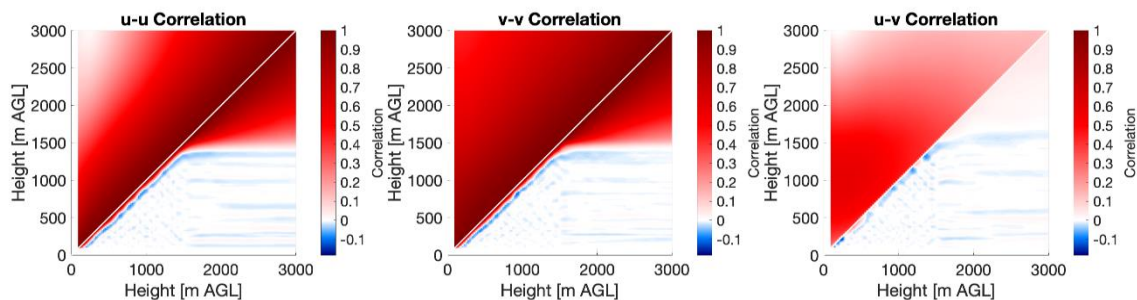
Figure 1: Correlation matrices for *u-u* (left), *v-v* (center), and *u-v* (right) for the month of July. The upper left half of each panel shows the correlation of the *a priori*, while the lower right half shows the correlation of the posterior for a clear-sky retrieval at 0235 UTC on 16 July 2019.
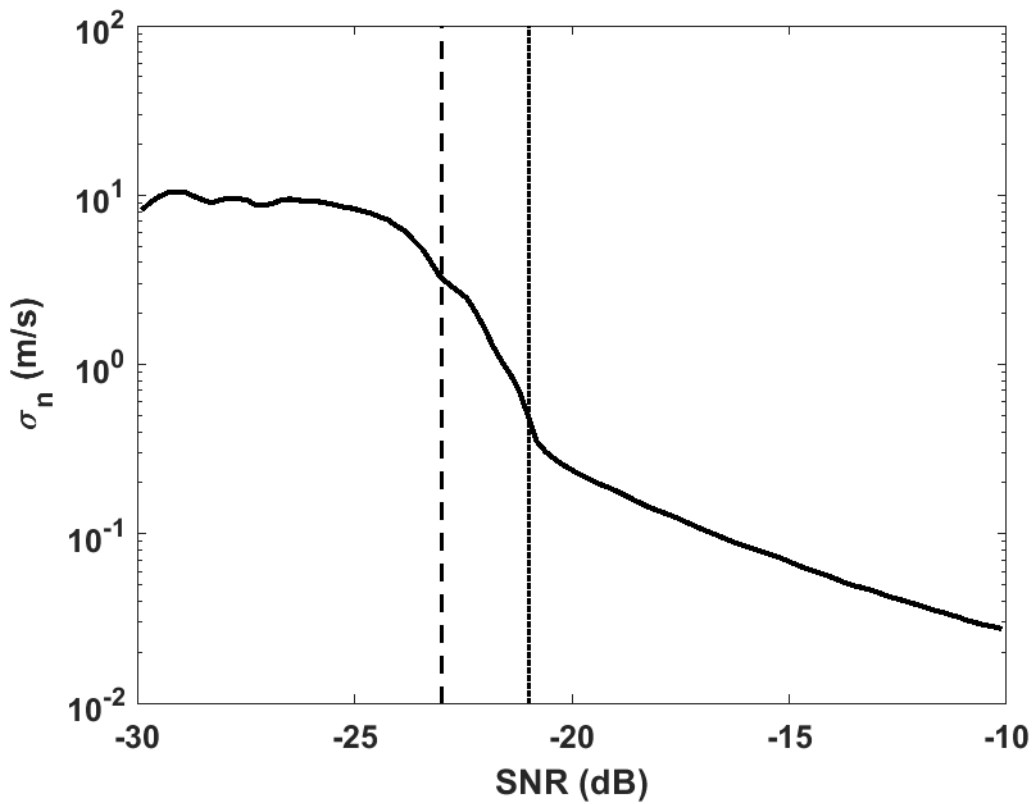
Figure 2: Measurement precision as a function of SNR for a day showing different SNR thresholds applied for VADtrad (dotted line) and VADoe retrievals (dashed line).
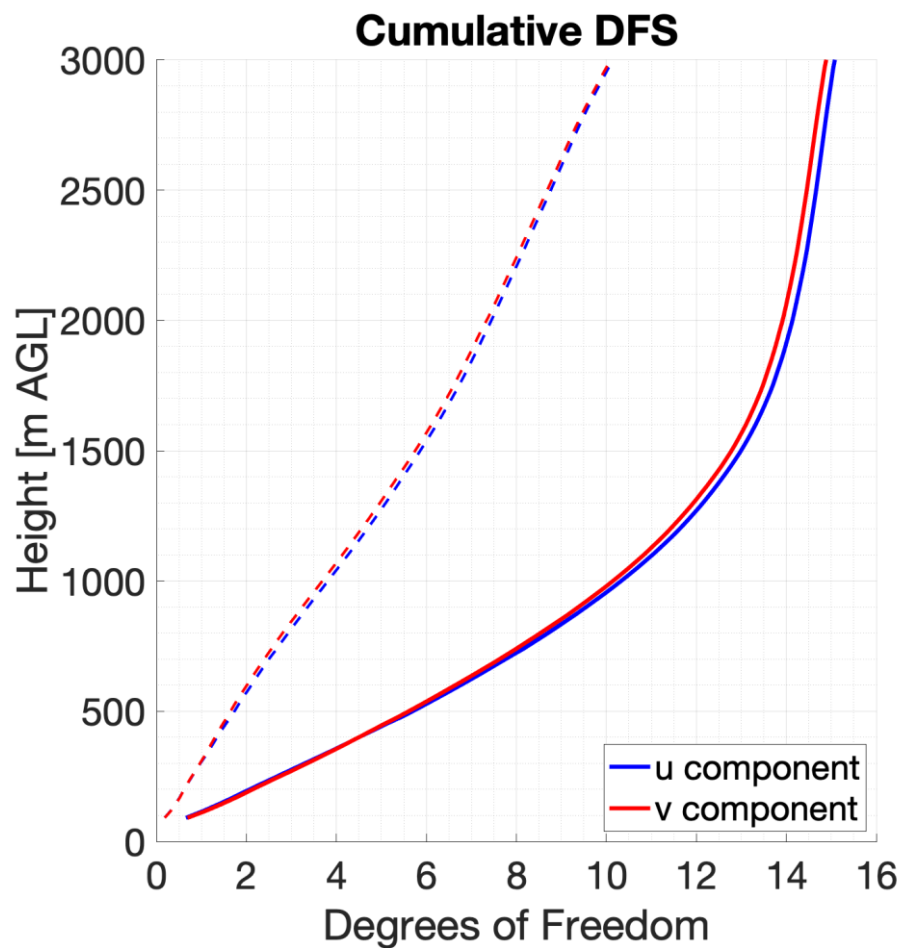
Figure 3. Vertical profile of the mean (solid) and 1-sigma (dashed) cumulative degrees of freedom of the signal calculated from the OE wind retrieval for both the *u* component (blue) and *v* component (red).

![Time-height cross sections showing v component of wind on 16 May 2019 with three panels: Traditional (top), Retrieval (middle), and Radiosondes (bottom)]
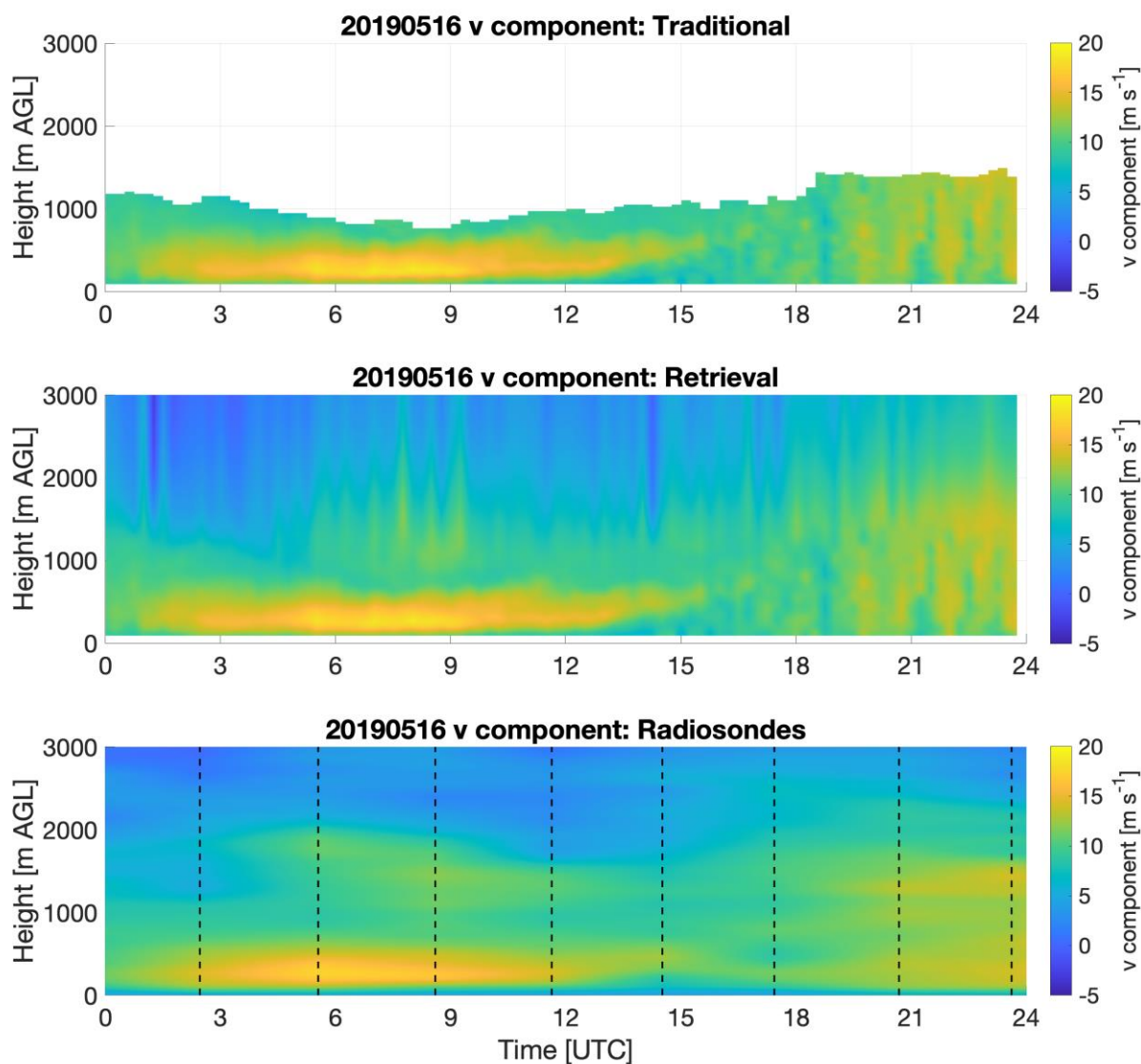
Figure 4: Time-height cross sections of the *v* component of the wind on 16 May 2019 as observed by VADtrad (top), VADoe (middle), and radiosonde (bottom). Radiosondes were launched every 3 h at the times indicated by dashed lines in the bottom panel. Time is in UTC; local time is UTC - 5.
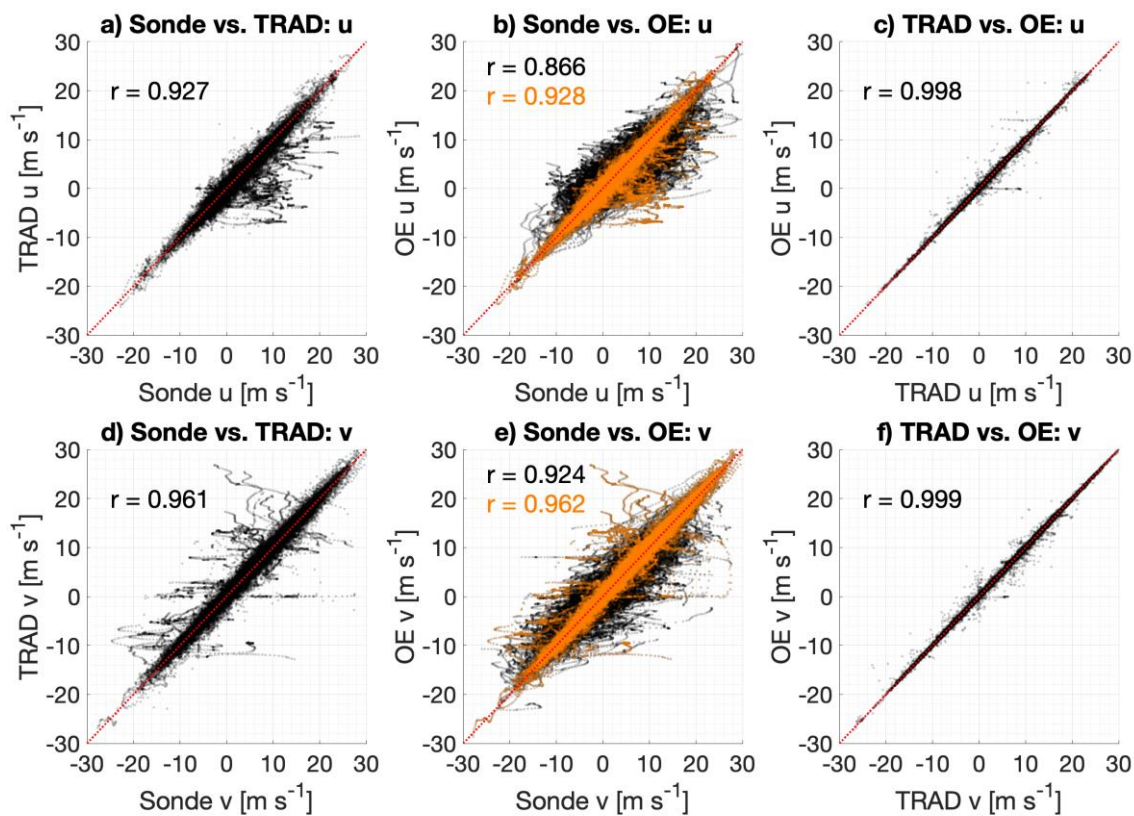
Figure 5: Scatter plots of the _u_ component (top row) and _v_ component (bottom row) of wind for radiosonde vs. VADtrad (left column), radiosonde vs. VADoe (center column), and VADtrad vs. VADoe (right column). The dotted red line represents the 1:1 line. Points in orange indicate the subset of VADoe observations for which a valid VADTrad observation also exists.
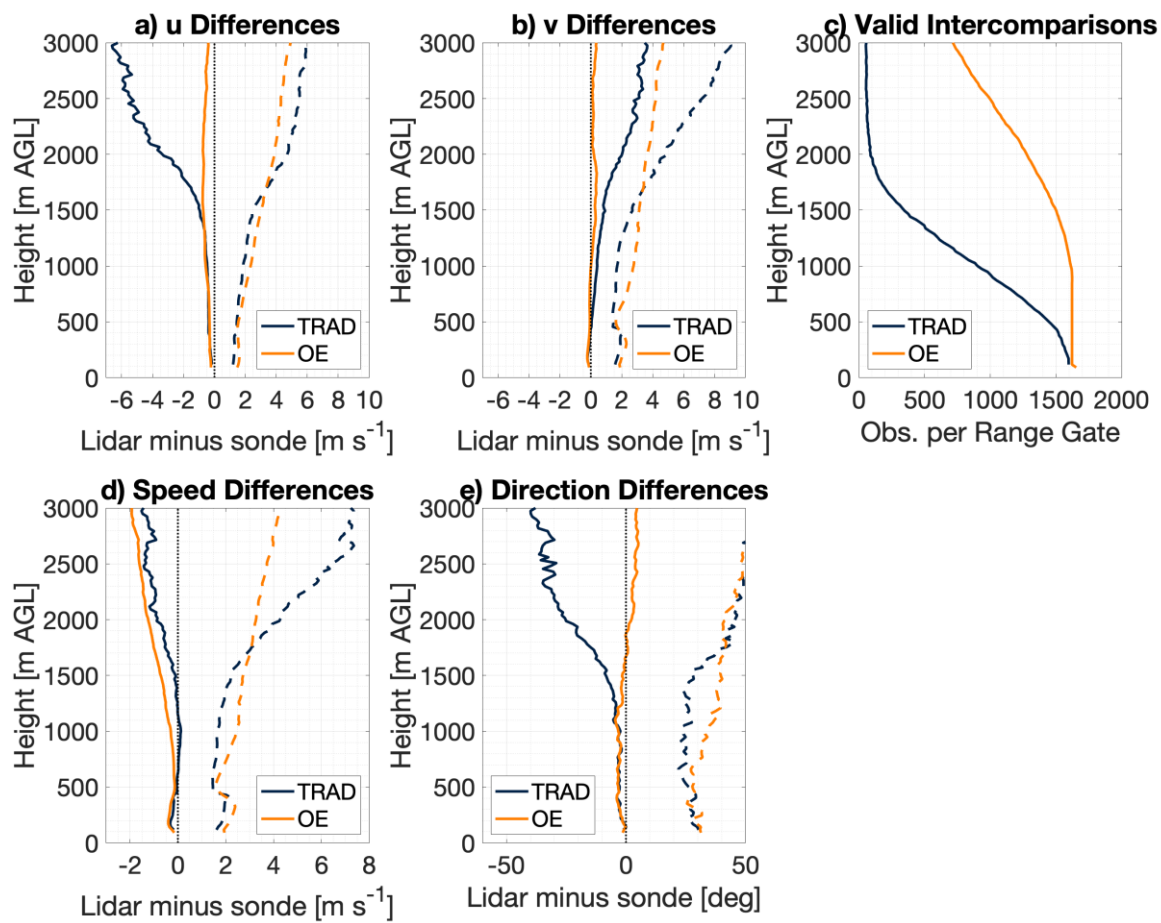
Figure 6: Vertical profiles of the bias (solid line) and 1-sigma uncertainty (dashed line) for VADoe (orange) and VADtrad (dark blue) for a) *u* winds in m s⁻ , b) *v* winds in m s⁻¹, d) wind speed in m s⁻¹, and e) wind direction in deg. Panel c) shows the number of valid intercomparisons as a function of height.
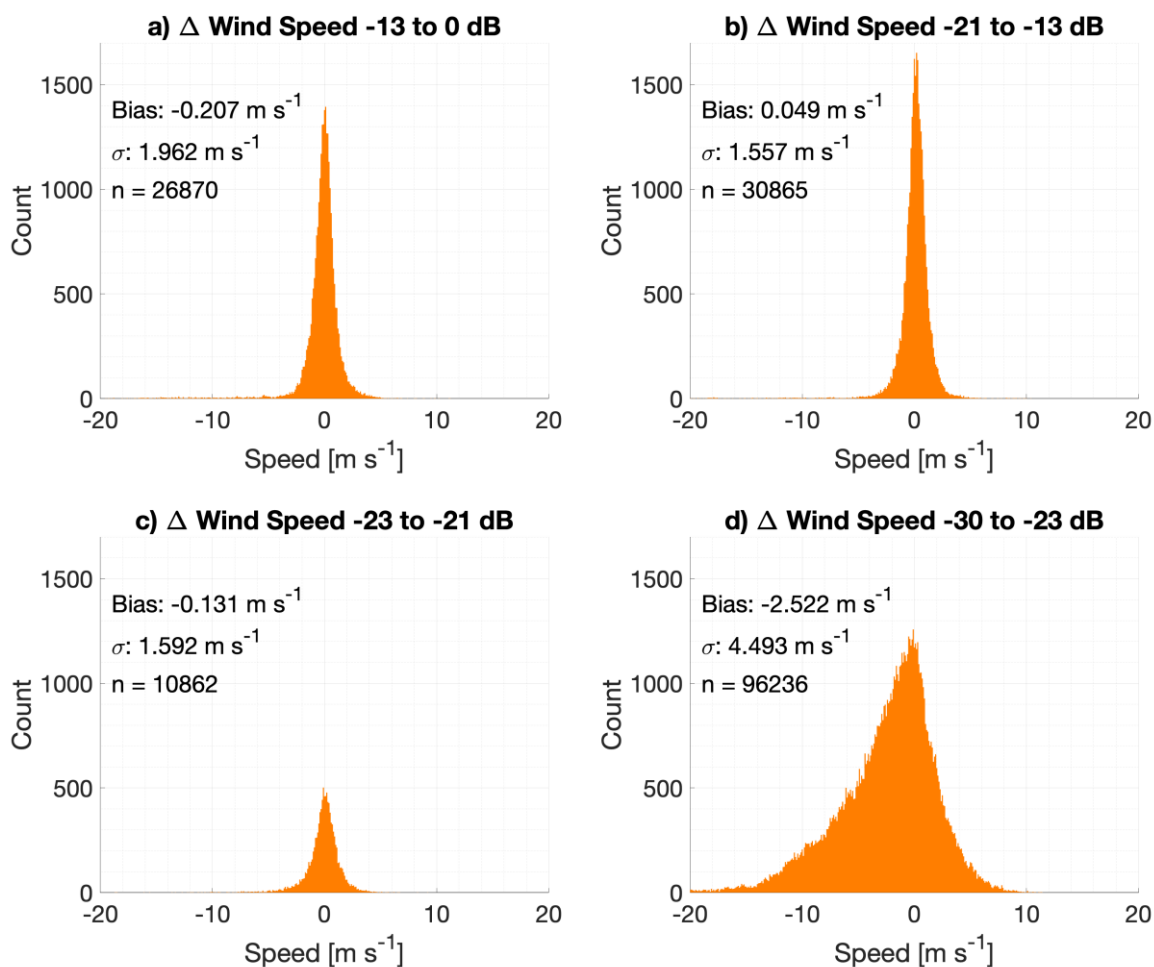
Figure 7: Histograms of the retrieval minus radiosonde differences in wind speed (in m s⁻¹) for four different bands of lidar signal to noise ratio.

475
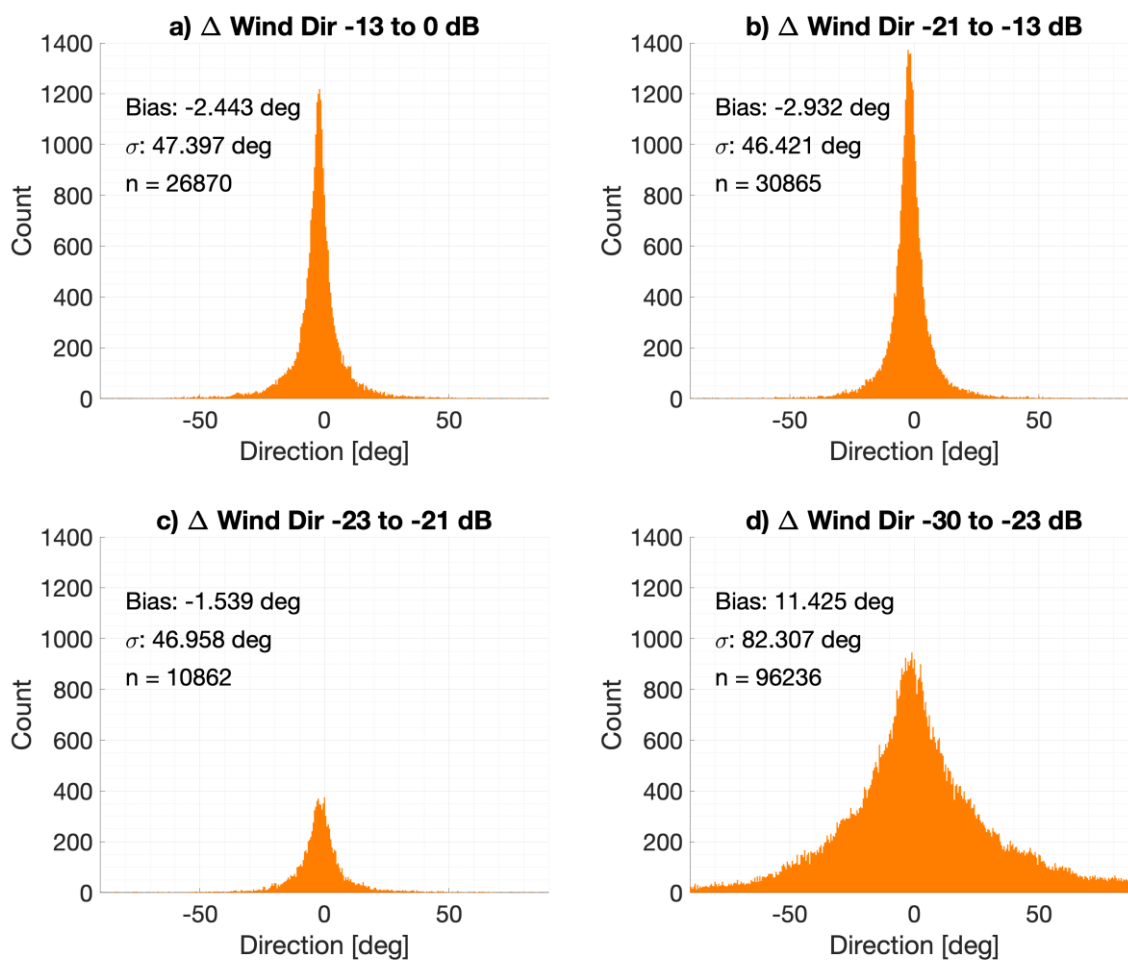
Figure 8: As in Fig. 7, but for wind direction (in degrees).